Progress In Electromagnetics Research, PIER 89, 39–56, 2009

AN IMPROVED TWO-SCALE MODEL WITH VOLUME SCATTERING FOR THE DYNAMIC OCEAN SURFACE

Z.-S. Wu, J.-P. Zhang, and L.-X. Guo

School of Science
Xidian University
Xi'an 710071, China

P. Zhou

National Electromagnetic Scattering Laboratory
Beijing 100854, China

Abstract—The effects of the surface slopes joint probability density, the shadowing function, the skewness of sea waves and the curvature of the surface on the backscattering from the ocean surface are discussed and an improved two-scale model modified by these four aspects is used to calculate the backscattering coefficient of the dynamic ocean surface. In order to deal with the surface skewness driven by wind, a new complementary term derived from the small perturbation method is included in the improved model, in which the Fourier transform of the third-order cumulant function, surface bispectrum, is employed. On this basis, with the oceanic whitecap coverage taken into account, a composite model for predicting the ocean surface backscattering coefficient is constructed tentatively, which incorporates the volume scattering into the total one. Finally, with the vector radiative transfer (VRT) theory employed, numerical illustrations are carried out for the backscattering coefficients versus wind speed, incidence angle and azimuth angle, respectively. The predictions of the composite model are verified in K_u- and K_a-bands through the comparison of numerical results with many sets of measured data and the aircraft measurement experiment carried out in ZHOUSHAN sea area also supports this model.

Corresponding author: Z.-S. Wu (wuzhs@mail.xidian.edu.cn).

1. INTRODUCTION

In the modeling of rough sea surface backscattering, two-scale model (TSM) is widely used [1–3]. In general, sea surface is made up of quasi-periodic large-scale wave and disordered foam, ripple and spray superposed on that, namely, it is composed of long gravity type sea waves that can have wavelengths of hundreds of meters and short capillary type sea waves that can have wavelengths in the millimeter range, and the small-scale roughness is distributed over the slope distribution of the large-scale roughness [4]. Kirchhoff approximation (KA) and small perturbation method (SPM) [5–7] are two basic approaches to calculate the scattering problem of rough surfaces which hold for the large-scale rough surface and the small-scale one, respectively. The classical two-scale method is developed from them. In order to describe the scattering from the ocean surface accurately, considerable effort has been devoted to the correction of many scattering models. Fung and Chen [5] used third-order statistics of the random surface to account for both surface slopes and skewness in surface heights in Kirchhoff model. Guissard [8] discussed the skewness function which depends on characteristic distances, introduced multispectra, and established relationships between these distances and the wind speed. Cox and Munk showed that the surface slope distribution is non-Gaussian, and introduced the Cox-Munk model [9]. Recently, Soriano et al. [10] replaced SPM with the small slope approximation to treat the small-scale roughness in the classical two-scale model, avoiding the difference brought by adopting different frequency cutoff. But for the crucial surface skewness correction, there has been no published paper since Wang et al. [11]. It is worth to note that the correction is not sufficient in that paper, especially in upwind direction. A new complementary term derived from the small perturbation method is introduced to TSM to describe the surface skewness in this paper. The curvature effect for $\theta_i > 70^\circ$, the shadowing effect, the skewness effect of sea waves and the slope distribution of the dynamic ocean surface are all considered in different models in published papers, respectively. In order to consider the total effect of these four aspects, the classical TSM is modified in this paper and the modified model is called four-modified two-scale model (FMTSM) temporarily.

In actual situations, wave breaking of the sea surface driven by strong wind appears, which results in much air is engulfed in the water forming a layer of air bubbles and part of the sea surface will be covered with foam which affects the scattering coefficient significantly. So the FMTSM is not accurate enough to calculate the sea surface

scattering. The contribution of the volume scattering of the foam must be considered. Droppleman [12] modeled the foam as a homogeneous layer with a mean dielectric constant. Rosenkratz and Staelin [13] presented a model of a series of plane, thin films parallel to the sea surface to estimate the effect of the foam layer to the radiate brightness temperature. Chen and Tsang et al. [14] treated the foam-covered ocean surface as densely packed air bubbles coated with thin layers of seawater, and applied Monte Carlo simulations of solutions of Maxwell's equations to calculate the absorption, scattering, and extinction coefficients. Jin et al. [15] presented a model of a layer of foam scatterers over a two-scale randomly rough sea surface. However, all these models are based on the classical TSM or others [16]. In this paper, the volume scattering of the foam is incorporated into the FMTSM tentatively, which is called the composite model, and the influence of the wind speed, the azimuth, the polarization and the foam coverage [17] are discussed quantitatively. Finally, the numerical results of the composite model and the classical model are compared with the experimental data.

2. FOUR CORRECTIONS TO THE OCEAN SURFACE BACKSCATTERING

For an incident plane wave in the x-z plane, the incoherent backscattering coefficient of an anisotropic non-Gaussian dynamic ocean surface derived from the classical TSM [11, 18] is shown as

$$\sigma_{hh}^{0s}(\theta_i) = \int_{-\infty}^{\infty}\int_{-\mathrm{ctg}\theta_i}^{\infty} (\hat{h}\cdot\hat{h}')^4\sigma_{hh}^{1s}(\theta_i')(1+z_x tg\theta_i)\times P(z_x,z_y)dz_x dz_y \quad (1)$$

$$\sigma_{vv}^{0s}(\theta_i) = \int_{-\infty}^{\infty}\int_{-\mathrm{ctg}\theta_i}^{\infty} (\hat{v}\cdot\hat{v}')^4\sigma_{vv}^{1s}(\theta_i')(1+z_x tg\theta_i)\times P(z_x,z_y)dz_x dz_y \quad (2)$$

where $\sigma_{hh}^{1s}(\theta_i')$ and $\sigma_{vv}^{1s}(\theta_i')$ are the first-order backscattering coefficient derived from the SPM for the HH and VV polarization, respectively. Other parameters are reported in [11].

The classical TSM is not robust in calculating the scattering from sea surface in actual situations; the real distribution of the surface slopes, the shadowing effect between surface facets, the effects of the surface skewness and curvature are not considered in it. For a more accurate result, these four corrections are incorporated into the classical two-scale model employing the sea spectrum developed by Fung [1] in this paper.

In Eq. (1) and Eq. (2) the large-scale roughness is described by KA, so the diffraction effect of the incident wave is neglected. For the low-grazing-angle, the large-scale portion of the rough sea surface should be considered as curved surface; namely, the modified factor of curvature $c_{pp}(\theta_i', k_iR)$ should be included. For the real rough sea surface, the roughness parallel to the wind direction is larger than the one perpendicular to it, so we only need to consider the curvature effect of large-scale roughness along the wind direction on the radar return. Let downwind direction be x-axis, the curvature radius R_x [19] in the modified curvature factors is shown as

$$R_x^2 = \int W(k_x, k_y) k_x^4 dk_x dk_y \tag{3}$$

where $W(k_x, k_y)$ is the two-dimensional sea spectrum.

In this paper, the backscattering coefficient derived from the SPM in Eq. (1) and Eq. (2) is modified by the factor given by Voronovich [21],

$$\sigma_{hh}(\theta_i') = c_{hh}(\theta_i', k_iR)[\sigma_{hh}(\theta_i')]_{R=\infty} \tag{4}$$

$$\sigma_{vv}(\theta_i') = c_{vv}(\theta_i', k_iR)[\sigma_{vv}(\theta_i')]_{R=\infty} \tag{5}$$

where $[\sigma_{hh}(\theta_i')]_{R=\infty}$ and $[\sigma_{vv}(\theta_i')]_{R=\infty}$ are backscattering coefficients without curvature effect derived from the SPM and the modified factor of curvature in Eqs. (4), (5) is.

$$c_{hh}(\theta_i', k_iR) = \frac{\left|\sqrt{\varepsilon_2 - \varepsilon_1 \sin^2\theta_i'} + \sqrt{\varepsilon_1}\cos\theta_i'\right|^4}{\left|\sqrt{\varepsilon_2 - \varepsilon_1 \sin^2\theta_i'}A^* + \sqrt{\varepsilon_1}\cos\theta_i' B^*\right|^4} \tag{6}$$

$$c_{vv}(\theta_i', k_iR) = \frac{\left|\varepsilon_1\sqrt{\varepsilon_2 - \varepsilon_1 \sin^2\theta_i'} + \varepsilon_2\sqrt{\varepsilon_1}\cos\theta_i'\right|^4}{\left|\varepsilon_1\sqrt{\varepsilon_2 - \varepsilon_1 \sin^2\theta_i'}A^* + \varepsilon_2\sqrt{\varepsilon_1}\cos\theta_i' B^*\right|^4} \tag{7}$$

with

$$A = \sqrt{\frac{\pi t}{2}} H_{1/3}^{(1)}(t) \exp\left(-it + i\frac{5\pi}{12}\right)$$

$$B = -\frac{i}{3\sin^2\theta_i'}\sqrt{\frac{\pi}{2t}}\left[(1 - 3it\cos^2\theta_i')H_{1/3}^{(1)}(t) + 3tH_{1/3}^{(1)'}(t)\right]\exp\left(-it + i\frac{5\pi}{12}\right)$$

$$t = \frac{1}{3}k_i\sqrt{\varepsilon_1}R\frac{\cos^3\theta_i'}{\sin^2\theta_i'}$$

The symbol $H_{1/3}^{(1)}(t)$ is the 1/3 order Hankel function of the first kind; ε_1 and ε_2 denote the permittivity of the air and sea water in this paper, respectively.

For large or low-grazing incidence angle, the incident and scattering shadowing of the sea surface are strong. However, since the shadow function of the non-Gaussian ocean surface is under investigation, the shadowing function for the Gaussian surface developed by Bourlier et al. [20] is employed in this paper,

$$S(v) = \frac{\Lambda'}{\Lambda + 1} \tag{8}$$

where

$$\Lambda' = 1 - \frac{\mathrm{erfc}(v)}{2}, \qquad \Lambda = \frac{\exp(-v^2) - v\sqrt{\pi}\mathrm{erfc}(v)}{2v\sqrt{\pi}} \tag{9}$$

with $v = \frac{\mu}{\sqrt{2}\sigma_x}$, $\mu = \cos\theta_i$, $\sigma_x^2 = \alpha + \varepsilon\cos(2\phi)$, $\alpha = \frac{\sigma_u^2+\sigma_c^2}{2}$, $\varepsilon = \frac{\sigma_u^2-\sigma_c^2}{2}$. σ_u and σ_c are the slope variances of the sea surface in upwind and crosswind direction respectively, calculated as

$$\sigma_u^2 = 3.16 \times 10^{-3} u_{12.5}, \qquad \sigma_c^2 = 0.003 + 1.92 \times 10^{-3} u_{12.5}$$

To illustrate the contribution of the curvature and shadowing effect to the backscattering, two comparisons of the backscattering coefficient predicted by the TSM modified by the curvature and shadowing effect with the prediction of the classical model are shown in Fig. 1. It is in upwind direction, and the frequency of the incident wave is 13.9 GHz. We can see from Fig. 1(a), in the case of hh polarization, the curvature effect results in the heightening of the level of the whole curve, i.e., the increase of the backscattering coefficient, but the shadowing effect is inconspicuous. In the case of vv polarization, both the curvature and shadowing effects result in the drop of the level of the whole curve, i.e., the decrease of the backscattering coefficient. Besides, the shadowing effect makes the curve increase slowly as the wind speed increases, which implies the roughness of the sea surface becomes larger and there is a strong shadowing effect. Despite the analysis in Eq. (8), the shadowing function is to be a constant approximately when the incidence angle does not exceed 60°, so the shadowing effect can be neglected. This behavior can be verified by Fig. 1(b). However, for the large incidence angle over 60°, the level of the shadowing function decreases gradually with the increase of the incidence angle, illustrating the strong shadowing effect. For the curvature modification, its contribution becomes low as the incidence angle decreases, indicated

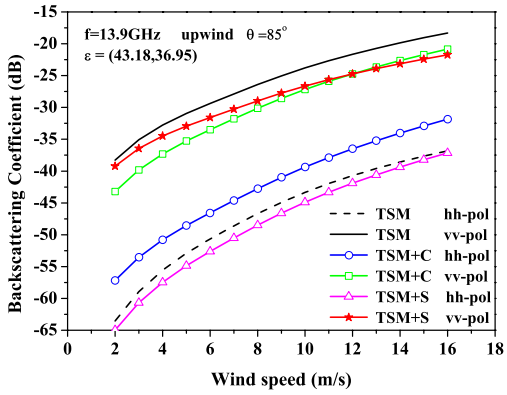

(a)

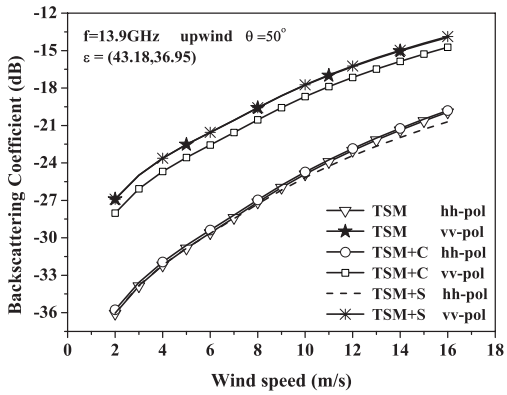

(b)

Figure 1. Illustration of the curvature and shadowing effect.

by the comparison of Fig. 1(a) with Fig. 1(b). The two corrections have much difference between *hh* and *vv* polarizations and the same conclusion can be drawn in the crosswind and downwind directions.

It is well-known that the backscattering coefficient measurement of the sea surface is asymmetry between upwind and downwind directions, which can be explained as the sea surface is skewed towards the direction of the wind. To illustrate the dependence on the sense of direction of the wind, the third-order statistics of the sea surface should be taken into account and the surface bispectrum should be introduced. We use the Fourier transform of the skewness function proposed by

Fung and Chen [5] to acquire the bispectrum,

$$S_a(\xi,\phi) = \left(\frac{\xi}{\sigma}\right)^3 \exp\left(-\frac{\xi^2}{s_0^2}\right)\cos^3\phi \tag{10}$$

Then, the imaginary part of the bispectrum $B_a(2k_i\sin\theta_i',\phi)$ [22] which represents the asymmetric effect of the ocean surface can be written as

$$B_a(K,\phi) = -\frac{Ks_0^6(6-K^2s_0^2\cos^2\phi)\cos\phi}{16}\times\exp\left(-\frac{K^2s_0^2}{4}\right) \tag{11}$$

It is worth to note that $K = 2k_i\sin\theta_i'$ is the spatial wavenumber; s_0 is the skewness distance similar to the correlation distance and ϕ is the azimuth angle relative to upwind direction.

For $\sigma_{hh}^{1s}(\theta_i')$ and $\sigma_{vv}^{1s}(\theta_i')$ in Eq. (1) and Eq. (2) backscattering coefficients are derived from the small perturbation model. We consider the skewness effect and include the surface bispectrum in the traditional SPM [22], which generates a complementary term to them after a mathematical implementation,

$$\sigma_{pp}^{2s}(\theta_i') = -16|\alpha_{pp}|^2k_i^5\cos^5\theta_i'\frac{B_a(K,\phi)}{K} \tag{12}$$

Note that the high order term of $\sigma_{pp}^{2s}(\theta_i')$ is dropped because we assume the multiple scattering is not important here. k_i is the electromagnetic wave number; θ_i' is the incidence angle in the local reference frame and α_{pp} is the polarization coefficient shown as

$$\alpha_{hh} = \frac{\varepsilon_r - 1}{[\cos\theta_i' + (\varepsilon_r - \sin^2\theta_i')^{1/2}]^2} \tag{13}$$

$$\alpha_{vv} = \frac{(\varepsilon_r-1)[(\varepsilon_r-1)\sin^2\theta_i' + \varepsilon_r]}{[\varepsilon_r\cos\theta_i' + (\varepsilon_r - \sin^2\theta_i')^{1/2}]^2} \tag{14}$$

Eq. (11) changes its value when the azimuth angle changes, which implies the existence of the skewness effect. Hence, to get a more accurate prediction of scattering from the skewed dynamic sea surface through the two-scale surface model, $\sigma_{hh}^{1s}(\theta_i')$ and $\sigma_{vv}^{1s}(\theta_i')$ in Eq. (1) and Eq. (2) should be substituted by $[\sigma_{hh}^{1s}(\theta_i') + \sigma_{hh}^{2s}(\theta_i')]$ and $[\sigma_{vv}^{1s}(\theta_i') + \sigma_{vv}^{2s}(\theta_i')]$, respectively.

In Eq. (1) and Eq. (2), the slope joint probability density function of the large-scale roughness which can not be defined easily is assumed to be Gaussian or Weibull distribution previously, but it does not

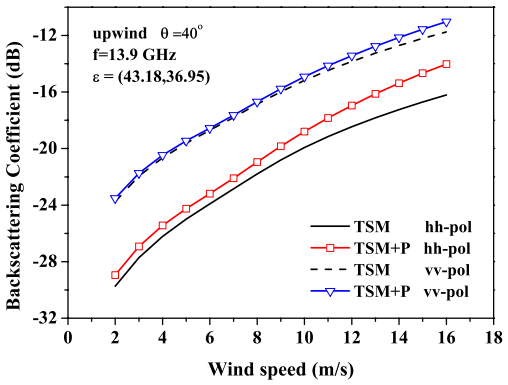

(a)

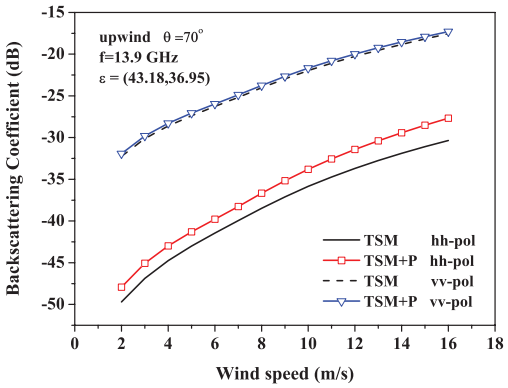

(b)

Figure 2. The effect of the correction of the surface slope probability density function.

hold for the real sea surface. In this paper, we employ the Cox-Munk's slick sea model [9], which describes the slope distribution of the ocean surface well in the upwind and downwind directions. The detailed theory description of the correction to the Cox-Munk's model is reported in reference [11].

In Fig. 2, a comparison of the backscattering coefficient predicted by TSM with and without the slope probability density correction is drawn; the frequency of incident wave is 13.9 GHz and the incidence angles are 40° and 70°. It is seen that the whole curve with the correction translates upward, indicating that the backscattering is enhanced. However, there are a few differences between the *hh* and *vv* polarizations. With the increase of the wind speed, the slope of the

curve becomes larger, which implies the strong effect of this type of correction in the hh polarization, but the contribution of the correction to the backscattering coefficient sustains a constant approximately in the vv polarization.

3. FMTSM

For an anisotropic dynamic ocean surface, the backscattering coefficient with a plane incident wave given by the improved TSM modified by these four aspects above, which is called FMTSM, is

$$\sigma_{hh}^{0s}(\theta_i) = S(v) \int_{-\infty}^{\infty}\int_{-\infty}^{\infty} (\hat{h}\cdot\hat{h}')^4 c_{hh}(\theta_i', k_i R_x) \cdot[\sigma_{hh}^{1s}(\theta_i')+\sigma_{hh}^{2s}(\theta_i')]_{R=\infty}\cdot(1+z_x \mathrm{tg}\theta_i)P(z_x,z_y)dz_x dz_y \quad (15)$$

$$\sigma_{vv}^{0s}(\theta_i) = S(v) \int_{-\infty}^{\infty}\int_{-\infty}^{\infty} (\hat{v}\cdot\hat{v}')^4 c_{vv}(\theta_i', k_i R_x) \cdot[\sigma_{vv}^{1s}(\theta_i')+\sigma_{vv}^{2s}(\theta_i')]_{R=\infty}\cdot(1+z_x \mathrm{tg}\theta_i)P(z_x,z_y)dz_x dz_y \quad (16)$$

where $\sigma_{hh}^{1s}(\theta_i')$ and $\sigma_{vv}^{1s}(\theta_i')$ are identical with the one in Eq. (1) and Eq. (2), shown as,

$$\sigma_{hh}^{1s}(\theta_i') = 8k_i^4 \cos^2\theta_i' |\alpha_{hh}|^2 W(2k_i \sin\theta_i', 0) \quad (17)$$

$$\sigma_{vv}^{1s}(\theta_i') = 8k_i^4 \cos^2\theta_i' |\alpha_{vv}|^2 W(2k_i \sin\theta_i', 0) \quad (18)$$

where θ_i and θ_i' are the incidence angles in the main and local reference frame, respectively; $P(z_x, z_y)$ is the modified slope distribution function of the large-scale wave slopes z_x and z_y; $\sigma_{hh}^{2s}(\theta_i')$ and $\sigma_{vv}^{2s}(\theta_i')$ are the additional terms accounting for the surface skewness; $c_{hh}(\theta_i', k_i R_x)$ and $c_{vv}(\theta_i', k_i R_x)$ are modified curvature factors which improve the two-scale model for large incidence angles; and $S(v)$ is the backscattering shadowing function.

The symbols α_{hh} and α_{vv} in Eqs. (17), (18) are the polarization coefficients [6], and $W(2k_i \sin\theta_i', 0)$ represents the sea spectrum.

In order to examine the validity of the FMTSM, comparisons of the backscattering coefficient among FMTSM, classical TSM and experimental measurements [23] are presented in Fig. 3. It is seen that the level of FMTSM is higher than that of classical model in upwind ($\phi = 0°, 360°$) and much lower in downwind ($\phi = 180°$). Besides, the level is different in the two directions that accounts for the asymmetric properties of the sea surface, but it is the same in the

classical model. And the minima of the curve are shifted from the crosswind direction ($\phi = 90°, 270°$) to the downwind direction. The predictions of FMTSM are in better agreement with experimental data than the classical model.

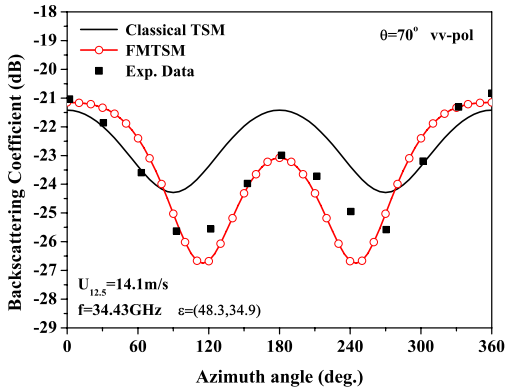

Figure 3. Comparisons of azimuthal behavior of the scattering curve between classical two-scale model, FMTSM and measurement at wind speed 14.1 m/s and polarization vv.

4. THE COMPOSITE MODEL BASED ON THE FMTSM

The FMTSM is better improved than the classical TSM. In order to describe the scattering more accurately, a composite model is constructed based on the very FMTSM in this paper. The composite model is of a layer of discrete spherical particles with underlying two-scale rough surface in the area of sea wave breaking, as shown in Fig. 4, in which the VRT theory is applied.

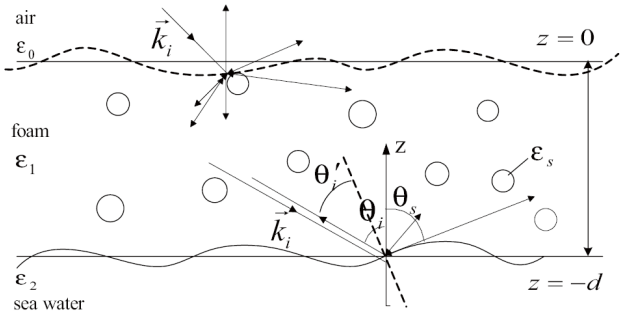

Figure 4. Geometry of the composite scattering model.

For simplicity, we assume the radius of the particle of foam is far smaller than the wavelength of the incident wave and the area of whitecap is a homogeneous foam layer overlying the slick sea surface. We use an iterative method to solve the vector radiation transfer (VRT) equation [24] of one foam layer with boundary conditions. First, we solve the VRT for the coherent solution when there is no multi-scattering. Then, the form-solution of the integral equation of VRT can be derived by using the constant variation method and boundary conditions. The zero-order backscattering coefficient derived from the zero-order solution of the VRT equation can be expressed as [15]

$$\begin{aligned}\sigma_{pq}^{(0)}(\theta_i) &= 4\pi\cos\theta_i \frac{I_{sp}^{(0)}(\theta_i, \pi+\phi_i)}{I_{0iq}(\pi-\theta_i, \phi_i)} \\ &= \cos\theta_i \gamma_{pq}(\theta_i, \pi+\phi_i; \pi-\theta_i, \phi_i) e^{-2\kappa_e d\sec\theta_i} \\ &= \sigma_{pq0}(\theta_i) e^{-2\kappa_e d\sec\theta_i} \end{aligned} \tag{19}$$

where the bistatic scattering coefficient is defined as

$$\gamma_{pq}(\theta, \phi; \theta_i, \phi_i) = \frac{4\pi\cos\theta I_{sp}(\theta, \phi)}{\cos\theta_i I_{iq}(\theta_i, \phi_i)} \tag{20}$$

I_{iq} and I_{sp} are the incident intensity and scattering intensity, respectively; $\sigma_{pq0}(\theta_i)$ is the backscattering coefficient of the rough foam-free sea surface. $e^{-2\kappa_e d\sec\theta_i}$ is the attenuation factor when the EM wave propagates in the layer of foam particles with thickness d.

Then, the first-order solution is obtained using an iterative method and the corresponding brief first-order backscattering coefficient is

$$\begin{aligned}\sigma_{hh}^{(1)}(\theta_i) &= \frac{3}{4}\cos\theta_i \frac{k_s}{k_e}\left(1 - e^{-2k_e d\sec\theta_i}\right)\cdot\left(1 + |R_{h0}|^4 \times e^{-2k_e d\sec\theta_i}\right) \\ &\quad + 3dk_s |R_{h0}|^2 e^{-2k_e d\sec\theta_i} \end{aligned} \tag{21}$$

$$\begin{aligned}\sigma_{vv}^{(1)}(\theta_i) &= \frac{3}{4}\cos\theta_i \frac{k_s}{k_e}\left(1 - e^{-2k_e d\sec\theta_i}\right)\left(1 + |R_{v0}|^2 e^{-2k_e d\sec\theta_i}\right) \\ &\quad + 3dk_s |R_{v0}|^2 e^{-2k_e d\sec\theta_i}\cos^2(2\theta_i) \end{aligned} \tag{22}$$

Note that k_s and k_e in Eq. (21) and Eq. (22) are the scattering and extinction coefficients of the foam particles, which are proportional to the fractional volume f_s,

$$f_s = \frac{3}{4} n_0 \pi a^3 \tag{23}$$

where a is the radius of spherical foam particles in millimeters and n_0 denotes the number of particles within a unit volume. R_{h0} and R_{v0}

are the Fresnel reflection coefficients of flat surface for horizontal and vertical polarization, respectively.

The sea surface is covered with foam partly under strong wind,

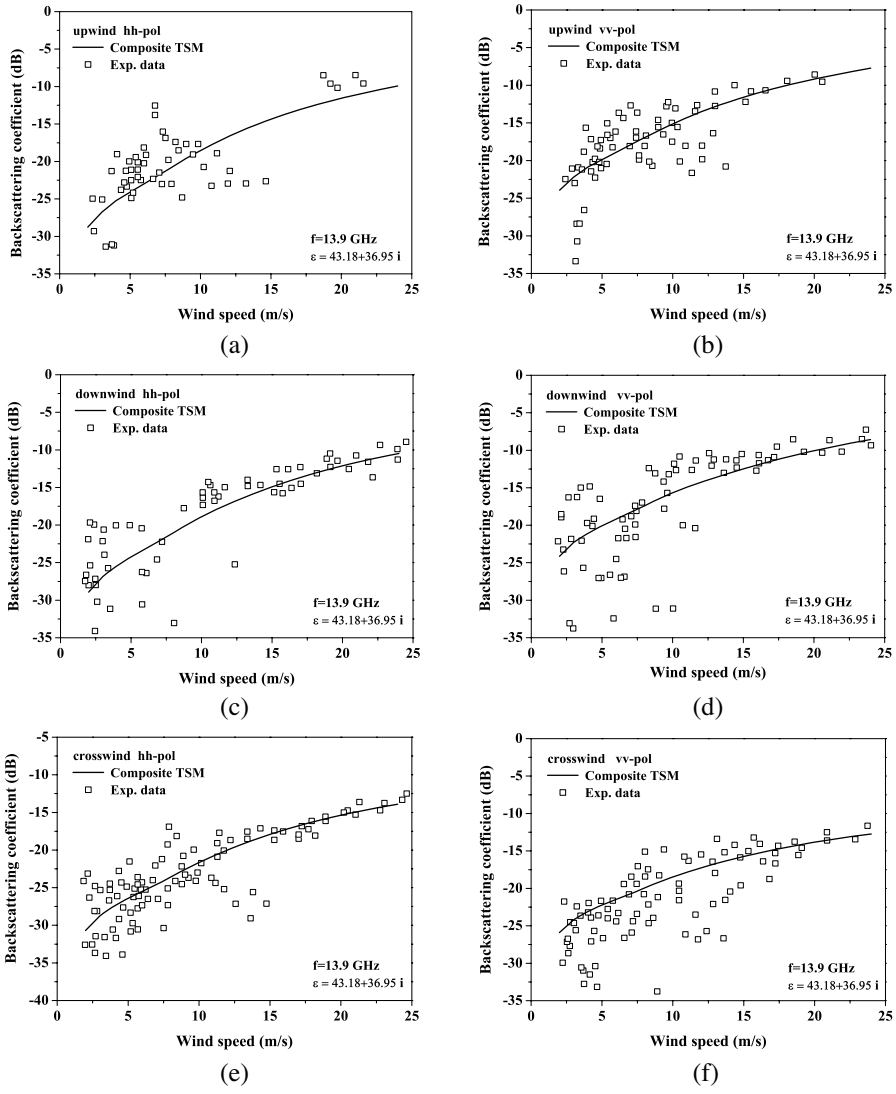

Figure 5. Comparisons of backscattering coefficient against wind speed between the composite model and measurement for incidence angle 40°.

so the total backscattering coefficient is contributed by the sea surface with and without foam.

$$\sigma_{hh}(\theta_i) = (1 - C_w)\sigma_{hh0}(\theta_i) + C_w(\sigma_{hh}^{(0)}(\theta_i) + \sigma_{hh}^{(1)}(\theta_i)) \quad (24)$$

$$\sigma_{vv}(\theta_i) = (1 - C_w)\sigma_{vv0}(\theta_i) + C_w(\sigma_{vv}^{(0)}(\theta_i) + \sigma_{vv}^{(1)}(\theta_i)) \quad (25)$$

where $\sigma_{hh0}(\theta_i)$ and $\sigma_{vv0}(\theta_i)$ are the backscattering coefficient of the foam-free sea surface calculated by Eq. (15) and Eq. (16); C_w denotes the foam coverage, which is expressed as [15],

$$C_w = 11.12e^{0.063u} - 16.23 \qquad (u \geq 7\,\mathrm{m/s}) \quad (26)$$

where u is the wind speed in meters per second at an altitude of 19.5 m above the sea horizon.

In Fig. 5, comparisons of the backscattering coefficient against wind speed between composite model including volume scattering of foam and experimental measurements [25] in three different wind directions are shown. The incidence angle is 40° and the foam coverage is calculated by Eq. (26) when the wind speed exceeds 7 m/s and assumed to be zero for 2 m/s∼7 m/s. The radius of foam particles is 1.1 mm and the thickness of foam layer is 4 cm. The level of the curve goes up as the wind speed increases, indicating more foams, high foam coverage and great contribution of volume scattering, but the slopes of curve become small gradually, which can be explained as there is a limit of the roughness and the foam coverage of the sea surface. Additionally, the backscattering coefficient decreases gradually for the same wind speed in upwind, crosswind and downwind directions, illustrating the influence of the sea surface skewness. Similar conclusions can be drawn for the incidence angles 25° and 55°.

The comparison of the backscattering coefficient predicted by the composite model and FMTSM with the experimental data is shown in Fig. 6, which illustrates the incidence angle dependence. The set of data is taken from the aircraft measurement experiment [26] which was carried out by the National Electromagnetic Scattering Laboratory in ZHOUSHAN sea area of China in 2003; the radar is VV polarization and the frequency is 17.16 GHz. Some meteorological conditions of the ocean are presented in Table 1. The temperature of the sea water is assumed to be 20°C and the salinity is chosen to be 35‰. The complex relative permittivity of sea water is $(39.9, -38.3)$. The assumed foam layer in calculation is 4 cm in thickness and the radius of foam particles is 1.1 mm. The predictions of the composite model in Figs. 6(a), (b) and Figs. 6(c), (d) are based on the ocean surface with a foam coverage 1.9% and 2.4%, respectively. It can be seen that the curve of the composite model has a better agreement with

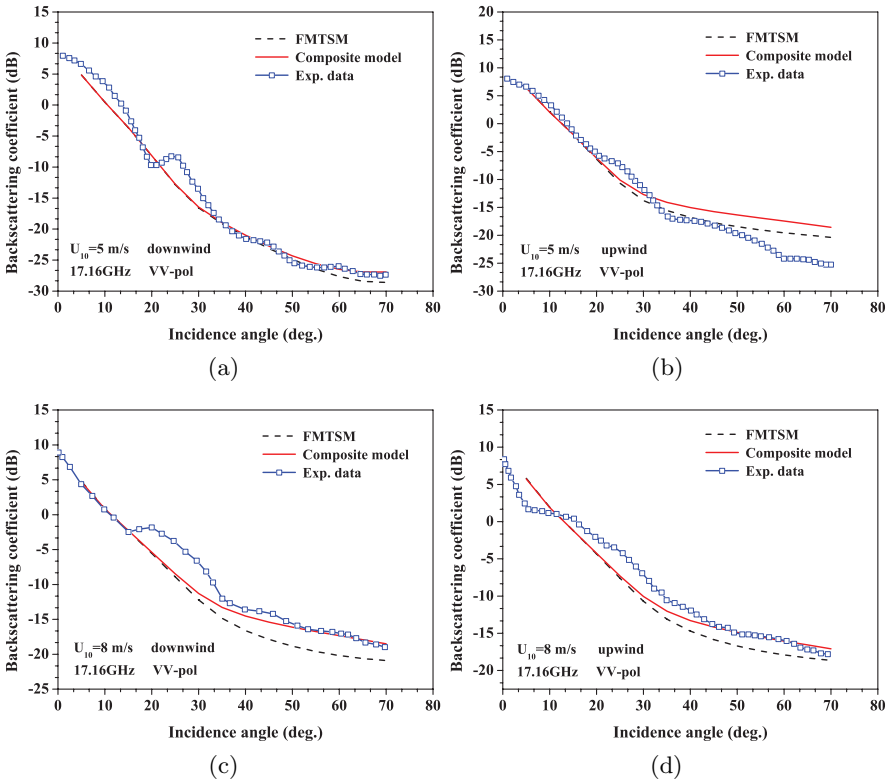

Figure 6. Illustration of the incidence angle dependence: (a, b) Nov. 14, $U_{10} = 5.0\,\mathrm{m/s}$ (c, d) Nov. 16, $U_{10} = 8.0\,\mathrm{m/s}$.

the experimental data than the FMTSM, except Fig. 6(b). Obviously, with the increase of the incidence angle, the discrepancy between the two models becomes larger, implying more contribution of the volume scattering to the total one, but the backscattering coefficient predicted by the two models is equivalent over the angular range from 5° to 20°. So we arrive at a conclusion as the following: the contribution of volume scattering becomes conspicuous with the increase of incidence angle, especially at large incidence angles. The foam effect must be considered in calculation of the backscattering from ocean surface.

Another comparison between FMTSM, composite model and measured data [23] is shown in Fig. 7 to illustrate the azimuth angle dependence at Ka-band, 34.43 GHz. The incidence angel is 70°. The complex relative permittivity of sea water is (48.3, −34.9) and the foam coverage is calculated by Eq. (26). The assumed thickness of the foam layer is 4 cm and the radius of foam particles is 1.0 mm. The wind

Table 1. Meteorological condition.

Date	Sea State Code	Wave Height in meter	Wind Direction	Wind Speed in m/s
Nov. 14	3	$0.8 \sim 1.5$	Lean to East	5.0
Nov. 16	4	$1.6 \sim 2.3$	Northeast	8.0

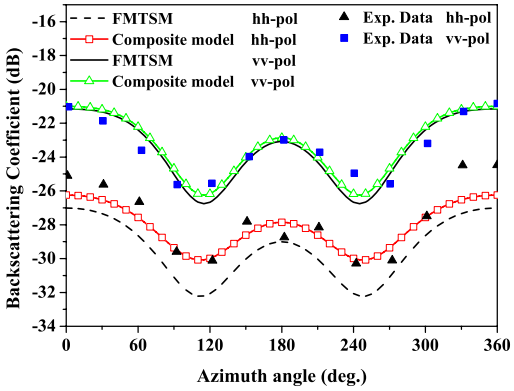

Figure 7. Comparisons of azimuthal behavior of the scattering curve between FMTSM, the composite model and experimental data, for incidence angle 70°.

speed is 14.1 m/s at an altitude of 12.5 m above the sea level. It is seen that the backscattering coefficient according to the composite model is in a close agreement with the measured data, and the correction degree of volume scattering of foam is deep in HH polarization, but it is very small in VV polarization. Note that the abscissa is the radar azimuth relative to the upwind direction. 0° and 180° correspond to the upwind and downwind directions, respectively. Obviously, the effect of volume scattering is significant in HH polarization, especially in crosswind direction, and the reason for the existent discrepancy in upwind direction is under investigation.

5. CONCLUSION

An improved two-scale model, the FMTSM, which is modified by four aspects, is proposed in this paper. The crucial consideration of the surface skewness effect with the new method in the two-scale model makes the predictions agree with the experimental data well. Further

more, a composite two-scale model including the volume scattering of foam based on the very FMTSM is presented tentatively with the VRT theory employed. The comparisons of the prediction between the classical TSM and FMTSM show that the results of the FMTSM fit experimental data well in K_a band. Additionally, some comparisons of FMTSM with the composite model are carried out, and the results indicate that the composite model has a good agreement with the experimental data. It is noted that the contribution of the volume scattering of the foam is high in K_a band and the high part of K_u band, but it is very low in the low part of K_u band, so the backscattering coefficient curves of the FMTSM and the composite model are not drawn in Fig. 5, simultaneously. The composite model for the more accurate predictions for other electromagnetic wave bands is under investigation.

ACKNOWLEDGMENT

This work is supported by the National Natural Science Foundation of China (Grant No. 60371020 and No. 60771038).

REFERENCES

1. Wright, J. W., "A new model for sea clutter," *IEEE Trans. Antennas Propagat.*, Vol. AP-16, No. 2, 217–223, 1968.
2. Valenzuela, G. R., "Theories for the interaction of electromagnetic and oceanic waves — A review," *Boundary-Layer Meteorology*, Vol. 13, 61–85, 1978.
3. Fung, A. K. and K. K. Lee, "A semi-empirical sea-spectrum model for scattering coefficient estimation," *IEEE J. Ocean. Eng.*, Vol. 7, No. 4, 166–176, 1982.
4. Fung, A. K. and N. C. Kuo, "Backscattering from multi-scale and exponentially correlated surfaces," *Journal of Electromagnetic Waves and Applications*, Vol. 20, No. 1, 3–11, 2006.
5. Fung, A. K. and K. S. Chen, "Kirchhoff model for a skewed random surface," *Journal of Electromagnetic Waves and Applications*, Vol. 5, No. 1, 205–216, 1991.
6. Ulaby, F. T., R. K. Moore, and A. K. Fung, *Microwave Remote Sensing-Active and Passive*, Vol. 2, Addision-Wesbey Pu. Co, 1982.
7. Tsang, L., J. A. Kong, and K. H. Ding, *Scattering of Electromagnetic Waves*, Vol. 1: Theory and Applications, Wiley-Interscience, New York, 2000.

8. Guissard, A., "Multispectra for ocean-like random rough surface scattering," *Journal of Electromagnetic Waves and Applications*, Vol. 10, 1413–1443, 1996.
9. McDaniel, S. T., "Microwave backscatter from non-Gaussian seas," *IEEE Trans. Geosci. Remote Sens.*, Vol. 41, No. 1, 52–58, 2003.
10. Soriano, G. and C. A. Guérin, "A cutoff invariant two-scale model in electromagnetic scattering from sea surfaces," *IEEE Trans. Geosci. Remote Sens.*, Vol. 5, No. 2, 199–203, 2008.
11. Wang, Y.-H., L.-X. Guo, and Z.-S. Wu, "Modified two-scale model for electromagnetic scattering from the non-Gaussian oceanic surface," *Chinese Physics Letters*, Vol. 22, No. 11, 2808–2811, 2005.
12. Droppleman, J. D., "Apparent microwave emissivity of sea foam," *J. Geophys. Res.*, Vol. 75, No. 3, 696–698, 1970.
13. Rosenkranz, P. W. and D. H. Stealin, "The microwave emissivity of ocean foam and its effect on nadiral radiometric measurements," *J. Geophys. Res.*, Vol. 77, No. 33, 6528–6538, 1972.
14. Chen, D., L. Tsang, et al., "Microwave emission and scattering of foam based on Monte Carlo simulations of dense media," *IEEE Trans. Geosci. Remote Sens.*, Vol. 41, No. 4, 782–790, 2003.
15. Huang, X.-Z. and Y.-Q. Jin, "Scattering and emission from two-scale randomly rough sea surface with foam scatterers," *IEE Proc. Microw. Antennas Propag.*, Vol. 142, No. 2, 109–114, 1995.
16. Guo, L.-X. and Z.-S. Wu, "Application of the extended boundary condition method to electromagnetic scattering from rough dielectric fractal sea surface," *Journal of Electromagnetic Waves and Applications*, Vol. 18, No. 9, 1219–1234, 2004.
17. Guo, J. J., L. Tsang, et al., "Applications of dense media radiative transfer theory for passive microwave remote sensing of foam covered ocean," *IEEE Trans. Geosci. Remote Sens.*, Vol. 39, No. 5, 1019–1027, 2001.
18. Chen, K. S., A. K. Fung, J. C. Shi, and H. W. Lee, "Interpretation of backscattering mechanisms from non-gaussian correlated randomly rough surfaces," *Journal of Electromagnetic Waves and Applications*, Vol. 20, No. 1, 105–118, 2006.
19. Smirnov, A. V., I. M. Fuks, and K. A. Naugolnykh, "Crosswind ocean radar backscatter and two-scale scattering model at low grazing angles," *Radio Science*, Vol. 38, No. 2, 8037–8044, 2003.
20. Bourlier, C., G. Berginc, and J. Saillard, "One and two-dimensional shadowing functions for any height and slope

stationary uncorrelated surface in the monostatic and bistatic Configurations," *IEEE Trans. Antennas Propag.*, Vol. 50, No. 3, 312–324, 2002.

21. Voronovich, A. G., "On the theory of electromagnetic waves scattering from the sea surface at low grazing angles," *Radio Science*, Vol. 31, No. 6, 1519–1530, 1996.
22. Chen, K. S. and A. K. Fung, "A Bragg scattering model for skewed sea surface," *OCEANS'90. 'Engineering in the Ocean Environment'. Conference Proceedings*, 249–252, 1990.
23. Chen, K. S., A. K. Fung, and D. E. Weissman, "A backscattering model for ocean surface," *IEEE Trans. Geosci. Remote Sens.*, Vol. 30, No. 4, 811–817, 1992.
24. Jin, Y.-Q., "Some results from the radiative wave equation for a slab of randomly, densely-distributed scatterers," *J. Quant. Spectr. Radiat. Transfer*, Vol. 39, No. 2, 83–98, 1988.
25. Schroeder, L. C., et al., "The relationship between wind vector and normalized radar cross section used to derive SEASAT-A satellite scatterometer winds," *J. Geophys. Res.*, Vol. 87, No. C5, 3318–3336, 1982.
26. Zhou, P., et al., "Results of airborne measurement of sea surface backscattering and analysis," *Systems Engineering and Electronics*, Vol. 28, No. 3, 325–328, 2006 (in Chinese).